NOTICE: When government or other drawings, specifications or other data are used for any purpose other than in connection with a definitely related government procurement operation, the U. S. Government thereby incurs no responsibility, nor any obligation whatsoever; and the fact that the Government may have formulated, furnished, or in any way supplied the said drawings, specifications, or other data is not to be regarded by implication or otherwise as in any manner licensing the holder or any other person or corporation, or conveying any rights or permission to manufacture, use or sell any patented invention that may in any way be related thereto.

U. S. Army Ordnance
Ballistics Research Laboratory
Aberdeen Proving Ground, Maryland
Approved Proposal No. 3175
Authorization No. 4086

EXPLOSIVES RESEARCH LABORATORY

HYPERVELOCITY IMPACT PHENOMENA

Quarterly Report
September 1, 1962 to November 30, 1962

BUREAU OF MINES, PITTSBURGH, PA.

UNITED STATES
DEPARTMENT OF
THE INTERIOR

HYPERVELOCITY IMPACT PHENOMENA

Quarterly Report

September 1, 1962 to November 30, 1962

Prepared for:

U. S. Army Ordnance
Ballistic Research Laboratory
Aberdeen Proving Ground, Maryland
Approved Proposal No. 3175
Authorization No. 4086

by

Richard W. Watson

Karl R. Becker

Frank C. Gibson

Approved by:

Robert W. Van Dolah, Chief
Explosives Research Laboratory

U. S. Department of the Interior
Bureau of Mines
Pittsburgh, Pa.
January 2, 1963

HYPERVELOCITY IMPACT PHENOMENA

Introduction

The purpose of this investigation is to study the parameters governing the failure of thin metal plates under the impact of high-speed fragments; special emphasis is placed on the lightweight structural alloys. The geometrical features of the perforations, together with the spatial, mass, and velocity distributions of the ejecta produced in the perforation process, are of immediate interest. Since these variables are strongly dependent on the characteristics of the impacting projectile as well as the physical properties of the target material, a variety of experimental approaches to the problem are clearly evident. In an effort to systematize the approach and at the same time gain information that will be of immediate practical value, a few select target materials are currently being investigated under impact conditions that involve the same projectile geometry but different impact velocities.

Behind-Target Effects

Spall Velocity Distribution Data

An experiment to determine the manner in which the velocities of spall fragments are distributed in the velocity spectrum has been initiated. The effort has met with some nominal success and, although quantitative features of the data sometime lack precision, they, along with certain other qualitative features, are of interest.

The greater portion of available data are from impacts with the Scale II projectiles; limited data from Scale I projectiles are also available. The projectile velocity was 3.2 km/sec. for both projectile scale sizes and in both cases the target material was 2024-T3 aluminum. Three different target thicknesses were investigated for each projectile size. The discussion deals with the experimental set-up and technique, comparison of the velocity distribution for different target thickness and fixed projectile size, a comparison of the velocity distributions between data from impacts with Scale II projectiles and Scale I projectiles, and a comparison of the velocity distributions for particles found at different radial distances measured from the center of impact.

The experimental technique for determining velocities and assigning velocity intervals to sub-groups of particles in the spall envelope involves the use of a framing camera; the equipment used in the experimental set-up is shown in figure 1. An explosive projector propells a projectile through a hole in a protective blast plate into a target of desired thickness. The envelope of spall from the bottom surface of the target plate is directed toward a lucite witness target whose top surface has been sprayed with black lacquer. The opaque surface is illuminated by a synchronized exploding wire; lighting efficiency is increased by enclosing the target-witness plate and wire in a white box. The framing camera views the bottom of the lucite plate by means of a 45° mirror. The impacting particles perforate the opaque

coating and are recorded as exposed spots on the film. The framing camera sequence is an accumulative record from which the arrival times of the spall particles are determined. A typical framing camera sequence is shown in figure 2.

The particles in the spall envelope can be subdivided into velocity intervals defined by the relationships:

$$v_n = \frac{S}{t + nt'} \quad (n = 0,1,2,\cdots) \tag{1}$$

$$\Delta v_n = v_{n+1} - v_n \tag{2}$$

where S = distance between target plate and witness plate;

t = time necessary for fastest particle to traverse S (determined independently by X-ray measurements);

t' = interframe time;

n = frame number.

It should be pointed out that the time t, which is the time required for the fastest particle to traverse distance S, was determined from a previous investigation of residual fragment velocities for Scale I impacts[1/].

Preliminary results, from a recent study at 3.2 km/sec., of residual fragment velocity for Scale II impacts indicate the applicability of a simple linear scaling law. That is, if the linear

---

1/ Quarterly Progress Report No. 24, "Fundamentals of Shaped Charges", Chapter III, Carnegie Institute of Technology, Contract No. DA-36-061-ORD-513, October 31, 1961.

dimensions of the projectile are scaled by a factor k, residual fragment velocities will be the same for the model and prototype if the target thickness is scaled by the same factor.

There may perhaps be some question regarding an error introduced by this technique due to the assumption that all particles have a common temporal origin. On the basis of a consideration of the projectile perforation time, the time necessary for multiple shock reflections to occur in the targets, and observations from framing camera records, the best estimate available is that a maximum error of ten percent is possible - for relatively thin targets the error is somewhat smaller.

The various plots, to be presented, take the form $\frac{1}{N}\frac{\Delta N}{\Delta v}$ vs $\bar{v}$ where ΔN is the difference between the number of particles observed to reside in two adjacent frames and Δv is the associated velocity interval as determined by equations (1) and (2). The reason for dividing ΔN by Δv is that equations (1) and (2) do not produce a series of equal Δv intervals and Δv serves as a weighting factor. The normalizing factor $\frac{1}{N}$, where N is the total number of particles, gives the coordinate $\frac{1}{N}\frac{\Delta N}{\Delta v}$ the property of a percentage. Hence, $\frac{1}{N}\frac{\Delta N}{\Delta v}$ vs $\bar{v}$ is interpreted to mean the relative percentage of the total number of spall particles having velocities within a velocity interval whose midpoint is $\bar{v}$.

The first data to be presented show $\frac{1}{N}\frac{\Delta N}{\Delta v}$ vs $\bar{v}$ for spall envelopes resulting from normal impacts by Scale II, 3.2 km/sec.

projectiles into three different target thicknesses of 2024-T3 aluminum. The data are plotted in figure 3 and summarized in table 1. The plot shows three distinct distributions; the distributions tend to shift in a direction corresponding to lower velocity values as the target thickness increases. The shift is noted for both the maximum spall velocity (intercepts with the $\bar{v}$ axis) and for the maxima of the curves ($\bar{v}$ corresponding to the maximum percentage of the total number). It should be mentioned at this point that each of the fragment distributions contain contributions from different sources; fragment remains, target particles carried along with projectile particles, and "true spall" particles resulting from shock interactions at the free surface of the target. Needless to say, the identification of these particles on a material basis is impossible by this technique. However it was hoped, at the onset of this experiment, that the framing camera technique might distinguish the true spall particles from other material if their individual velocity distributions were sufficiently distinct (one would obtain multimodal distributions); this is apparently not the case for the 1/8-inch and 1/4-inch thick targets. The data from 3/8-inch thick targets do have a tendency toward the bimodal form and one would be inclined to consider the rather marginal evidence as being not significant were it not for somewhat similar results obtained in another set of data. The other set of data are shown in figure 4 and are tabulated in table 2. The experimental conditions are essentially the same for these data except that roughly 80% of the total

number of particles, having lower penetration capabilities, have been trapped in an 8-mil thick aluminum foil placed on the witness target. The plot shows $\frac{1}{N}\frac{\Delta N}{\Delta v}$ vs $\bar{v}$ for the same three target thicknesses and qualitatively, a comparison between the three thickness groups in figure 4 is similar to that given for figure 3. A comparison of corresponding thicknesses between the two figures reveals that a greater proportion of the low velocity particles have been filtered out because the maxima of the curves for the 1/8 inch and 1/4 inch targets in figure 4 have been shifted to the right (in a direction corresponding to a higher velocity value). This is not particularly noticeable for the 3/8 inch targets. The distribution for the 3/8 inch targets however, continue to show the bimodal form and assuming that the velocity distributions for the "true spall" and projectile remnants are sufficiently distinct, one would associate the left peak with true spall and the right peak with projectile remnants and associated target material.

Figure 5 compares the "Scale II" data from figure 3 with similar data obtained from impacts with Scale I projectiles. It is to be recalled that the Scale II projectile is a 1/8 inch diameter x 1/8-inch long, steel, cylinder having a mass of roughly 200 mg. whereas the Scale I projectile is a steel cylinder 1/16 inch diameter x 1/16 inch long having a mass of roughly 25 milligrams. Both projectile velocities were 3.2 km/sec. The target thicknesses for the Scale I impacts were 1/16 inch, 1/8 inch, and 3/16 inch as compared to 1/8

inch, 1/4 inch, and 3/8 inch for Scale II impacts. Hence, the set of target thicknesses for the Scale I impacts have been scaled down by a factor of two. The Scale I data are summarized in table 3. The three curves on the plot are the Scale II results from figure 3 and the data points shown are from, somewhat limited, Scale I results. The designation "f" is the scale factor which is equal to two for Scale II data and equal to one for Scale I data.

The purpose of the comparison is to see if the velocity distributions, obtained from Scale I and Scale II impacts, compare on a scaled target thickness basis rather than on an equal target thickness basis. The former appears to be the more likely basis for comparison; e.g., the particular Scale I data points designated by stars are for Scale I projectiles impacting 3/16-inch thick targets and these data points have a tendency to fit the Scale II curve designated by $\frac{t}{f} = 3/16$ ($f = 2$, so these are actually 3/8 inch targets impacted by Scale II projectiles). If the velocity distribution curves were comparable on an equal target thickness basis, then the stars would be required to fit a curve (for which there is no data) that would lie between those designated by $\frac{t}{f} = 1/8$ and $\frac{t}{f} = 1/16$; this is out of the question, and it appears that a comparison on a scaled target thickness basis is the more reasonable assumption. Further evidence in favor of comparing curves on a scaled target thickness basis is furnished by the fit between solid circles (Scale I projectiles impacting 1/16-inch thick targets) and the curve designated by $\frac{t}{f} = 1/16$ (Scale II

projectiles impacting 1/8 inch targets). A possible third comparison, the one between data points indicated by crosses and the curve designated by $\frac{t}{f} = 1/8$ does not furnish any information one way or the other. The plot suggests that the velocity distributions scale directly with the linear dimensions of the projectile only if the target thickness is scaled correspondingly.

A comparison has been made between the velocity distributions for spall particles located at various radial distances from the center of spall impact. The data are summarized in table 4 and are plotted in figure 6. The plot shows $\frac{1}{N}\frac{\Delta N}{\Delta v}$ vs $\bar{v}$ for four different radial distances from the center of impact; these distances are defined by the angular parameter θ_1 (sometimes referred to as the displacement angle). The angle θ_1 is the angle between a target normal and the trajectory of the particle considered. The distributions are from Scale II projectiles impacting 1/4-inch thick aluminum 2024-T3 targets. The data have been corrected for differences in path lengths. The comparison indicates that, (1) the maxima of the curves are roughly similar in that they observed to lie between 600 and 800 m/sec.; i.e., there is no definite correlation between the v where the maxima is observed and θ_1; (2) there is a correlation between the fastest fragment in each group (intercept with the $\bar{v}$ axis) and θ_1 with the velocity of the fastest fragment decreasing as θ_1 increases. This behavior is probably due to the relatively fewer projectile remnants (the projectile remnants, in general, have higher velocities than target spall material) that move outward at large dispersion angles.

Summary of Behind-Target Effects

(1) This portion of the report describes a technique for determining the distribution of spall velocities. The technique makes use of a framing camera and the sequence of pictures allows one to separate the total number of spall particles into groups having characteristic velocities within a velocity interval v and $v + \Delta v$. The technique can be used independently or to supplement a technique which determines spall velocities in terms of their depth of penetration into a calibrated target.

(2) A comparison of velocity distribution curves for different thicknesses of aluminum 2024-T3 targets impacted by Scale II, 3.2 km/sec. projectiles, show the expected shift of the curves in the direction of lower velocity values as the target thickness is increased. The distribution for relatively thick targets tends to show the bimodal form which probably arises from a resolution between the velocities of projectile remnants (and/or target material driven through the perforation) and spallation resulting from shock interactions at the free surface of the target.

(3) A comparison between the velocity distributions obtained from tests with two different projectile scale sizes shows that the velocity distributions are similar for target thicknesses scaled in the same ratio as the projectile dimensions.

(4) A comparison of velocity distributions between groups of spall particles striking the witness plate at different radial distances

from the center of impact shows that the velocity corresponding to the maximum number of spall particles is not significantly different between the groups despite the fact that there is a correlation between the highest fragment velocity in each group and the groups radial coordinate.

Table 1. - Distribution of spall velocities for spall particles produced by Scale II projectiles impacting aluminum 2024-T3 targets.

t = 1/8 in.		t = 1/4 in.		t = 3/8 in.	
$\frac{1}{N}\frac{\Delta N}{\Delta v}$	$\bar{v}$ (m/sec)	$\frac{1}{N}\frac{\Delta N}{\Delta v}$	$\bar{v}$ (m/sec)	$\frac{1}{N}\frac{\Delta N}{\Delta v}$	$\bar{v}$ (m/sec)
2.3	1960	2.4	1380	10.3	530
2.8	1310	5.8	920	33.4	450
9.6	900	18.8	590	22.4	340
6.4	520	6.2	330	26.9	240
5.4	290	2.0	200	4.7	170
2.1	200	-	-	-	-

Notes: (1) t is the thickness of aluminum 2024-T3 target material impacted by Scale II projectiles at normal incidence.

(2) ΔN is the number of spall particles having velocities in the velocity interval Δv and $\bar{v}$ is the midpoint of that interval.

(3) N is the total number of spall particles produced for a particular target thickness group.

Table 2. - Distribution of spall velocities for spall particles produced by Scale II projectiles impacting aluminum 2024-T3 targets. The distribution is for the 20 percentile group of spall particles having the highest penetration capabilities

t = 1/8 in.		t = 1/4 in.		t = 3/8 in.	
$\frac{1}{N}\frac{\Delta N}{\Delta v} \times 10^4$	$\bar{v}$ (m/sec)	$\frac{1}{N}\frac{\Delta N}{\Delta v} \times 10^4$	$\bar{v}$ (m/sec)	$\frac{1}{N}\frac{\Delta N}{\Delta v} \times 10^4$	$\bar{v}$ (m/sec)
3.2	2250	4.8	1460	24.8	500
6.5	1870	9.7	1200	19.8	400
6.5	1520	10.8	960	20.3	340
5.6	1240	13.5	780	13.8	280
3.4	980	11.2	640	9.4	230
6.1	780	4.0	270	15.6	200
3.3	630	3.3	180	17.2	170
-	-	-	-	36.4	150
-	-	-	-	30.9	140

Notes: (1) t is the thickness of aluminum 2024-T3 target material impacted by Scale II, 3.2 km/sec. projectiles at normal incidence.

(2) ΔN is the number of spall particles having velocities in the velocity interval Δv and $\bar{v}$ is the midpoint of that interval.

(3) N is the total number of spall particles produced for a particular target thickness group.

Table 3. - Distribution of spall velocities for spall particles produced by Scale I projectiles impacting aluminum 2024-T3 targets

t = 1/16 in.		t = 1/8 in.		t = 3/16 in.	
$\frac{1}{N}\frac{\Delta N}{\Delta v} \times 10^4$	$\bar{v}$ (m/sec)	$\frac{1}{N}\frac{\Delta N}{\Delta v} \times 10^4$	$\bar{v}$ (m/sec)	$\frac{1}{N}\frac{\Delta N}{\Delta v} \times 10^4$	$\bar{v}$ (m/sec)
1.2	2250	3.8	1530	9.1	620
2.0	1980	6.9	1400	19.5	510
4.9	1680	8.3	1240	26.0	390
5.5	1340	9.7	1080	30.6	270
9.7	1050	9.6	930	29.3	200
11.0	800	9.5	780	-	-
-	-	17.0	630	-	-

Notes: (1) t is the thickness of aluminum 2024-T3 target material impacted by Scale II, 3.2 km/sec. projectiles at normal incidence.

(2) ΔN is the number of spall particles having velocities in the velocity interval Δv and $\bar{v}$, is the midpoint of that interval.

(3) N is the total number of spall particles produced for a particular target thickness group.

Table 4. - Velocity spectra for spall particles located at different radial distances out from the center of impact. The data is for Scale II projectiles impacting aluminum 2024-T3 targets

(θ_1 = 0° - 9°)		(θ_1 = 9° - 17°)		(θ_1 = 17° - 25°)		(θ_1 = 25° - 32°)		(θ_1 = 32° - 38°)	
$\frac{1}{N}\frac{\Delta N}{\Delta V} \times 10^4$	$\bar{V}$ (m/sec)	$\frac{1}{N}\frac{\Delta N}{\Delta V} \times 10^4$	$\bar{V}$ (m/sec)	$\frac{1}{N}\frac{\Delta N}{\Delta V} \times 10^4$	$\bar{V}$ (m/sec)	$\frac{1}{N}\frac{\Delta N}{\Delta V} \times 10^4$	$\bar{V}$ (m/sec)	$\frac{1}{N}\frac{\Delta N}{\Delta V} \times 10^4$	$\bar{V}$ (m/sec)
4.7	1200	3.3	1410	7.6	1100	3.7	1170	2.5	990
6.8	700	9.9	860	11.8	810	15.9	790	22.1	770
11.0	440	7.0	460	11.9	530	6.4	480	14.7	560
9.6	280	5.8	260	6.3	290	4.5	290	6.5	330

Notes: (1) The coordinate θ_1 is the angular measurement between the line of flight of the projectile and the direction in which a particular portion of the spall envelope travels.

(2) ΔN is the number of spall particles having velocities in the velocity interval Δv.

(3) N is the total number of spall particles in the particular θ_1 space interval specified.

(4) The spall was produced by Scale II, 3.2 km/sec. projectiles impacting 1/4 inch aluminum 2024-T3 targets at normal incidence.

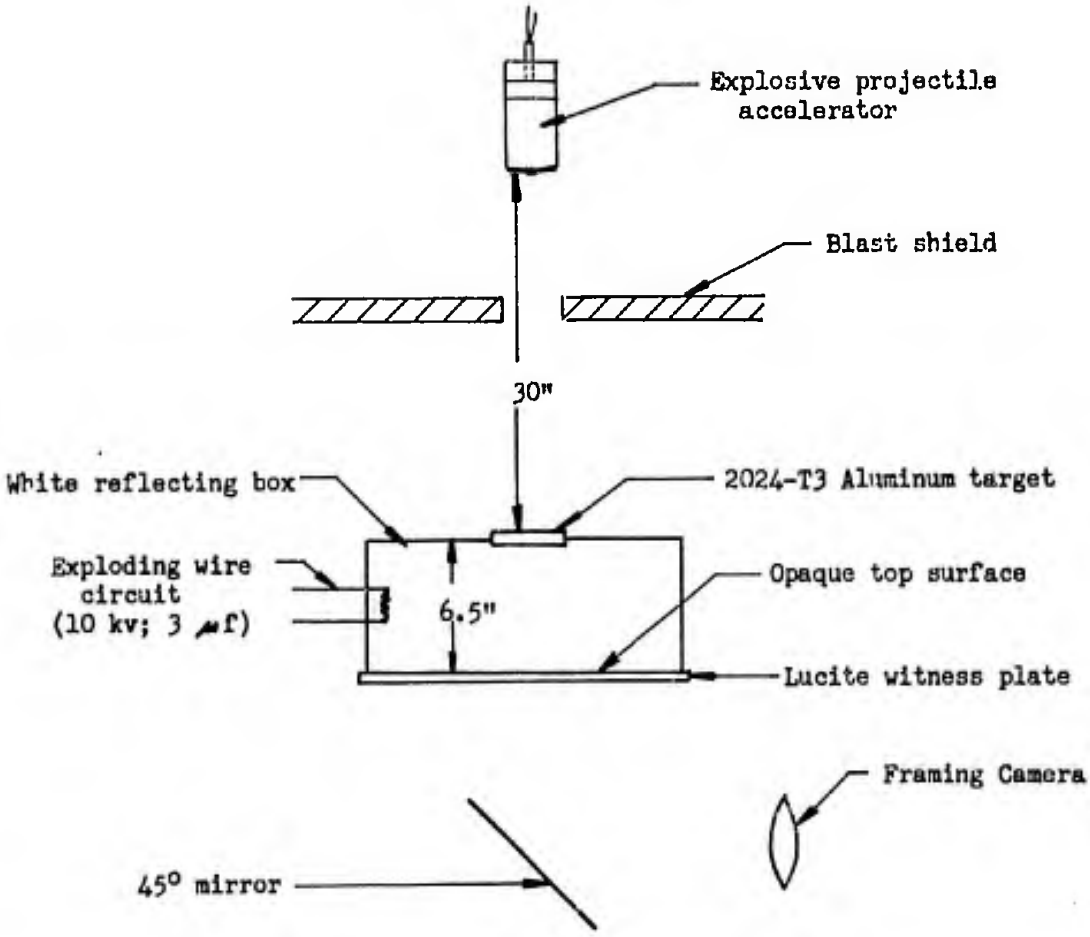

Fig. 1 The experimental apparatus used for obtaining measurements from which the distributions of spall velocities were determined.

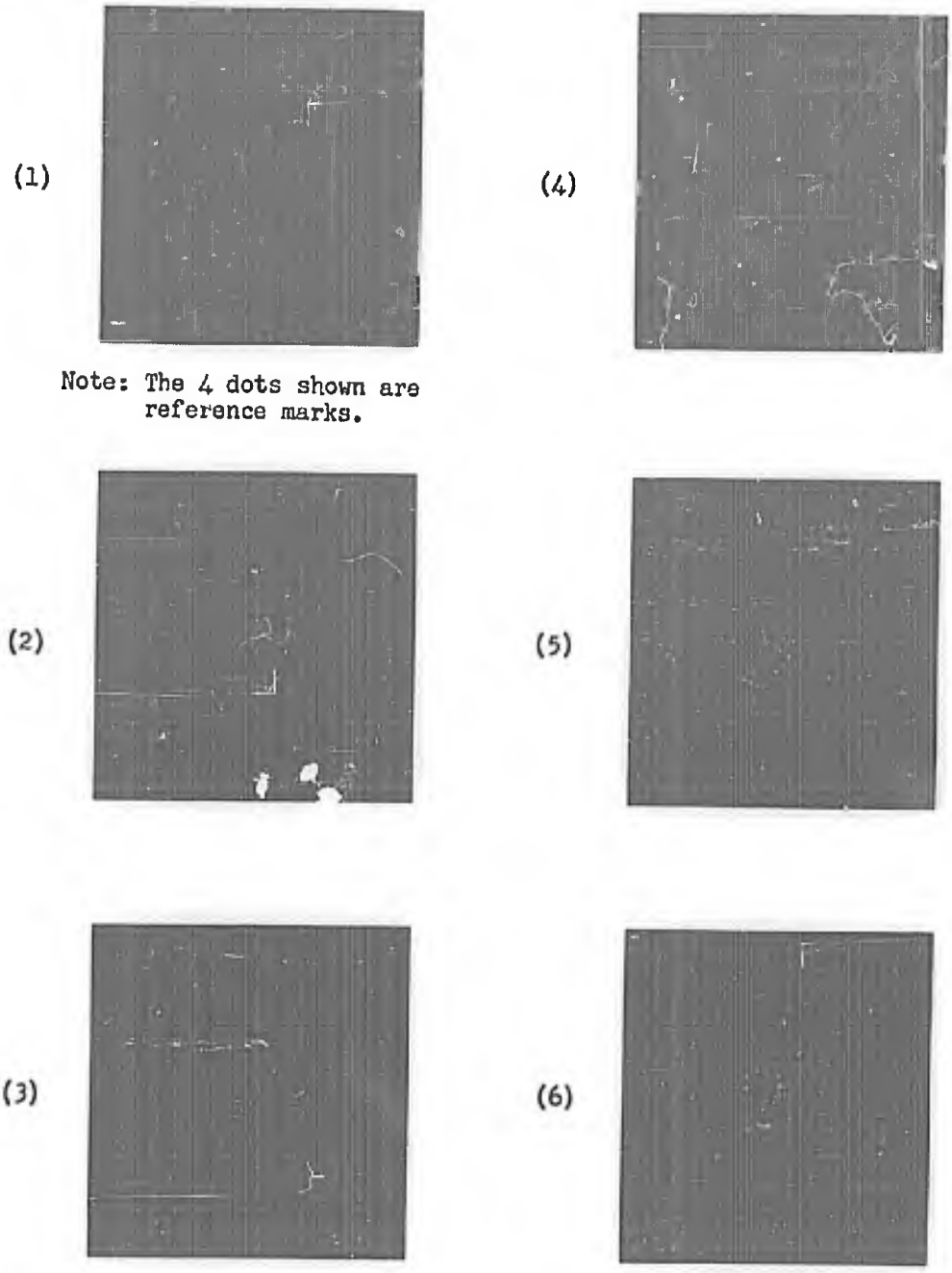

Fig. 2 Typical frames from a framing camera sequence of pictures used to determine the distribution of spall velocities.

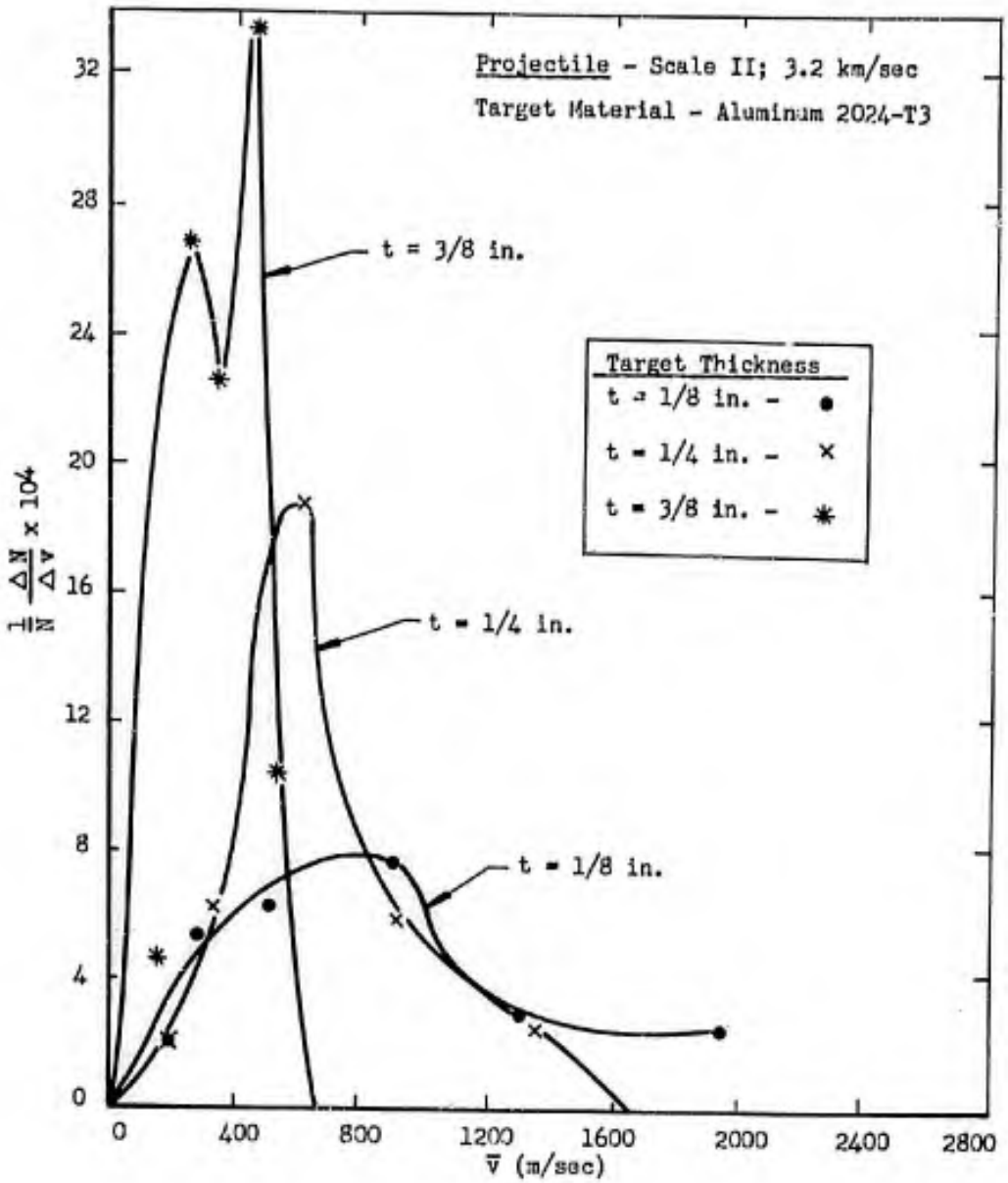

Fig. 3 Velocity spectrum distribution of spall particles, produced by impacts with Scale II projectiles into aluminum targets. The plot shows essentially the percentage of the total number of spall particles having velocities within velocity intervals defined by midrange data points.

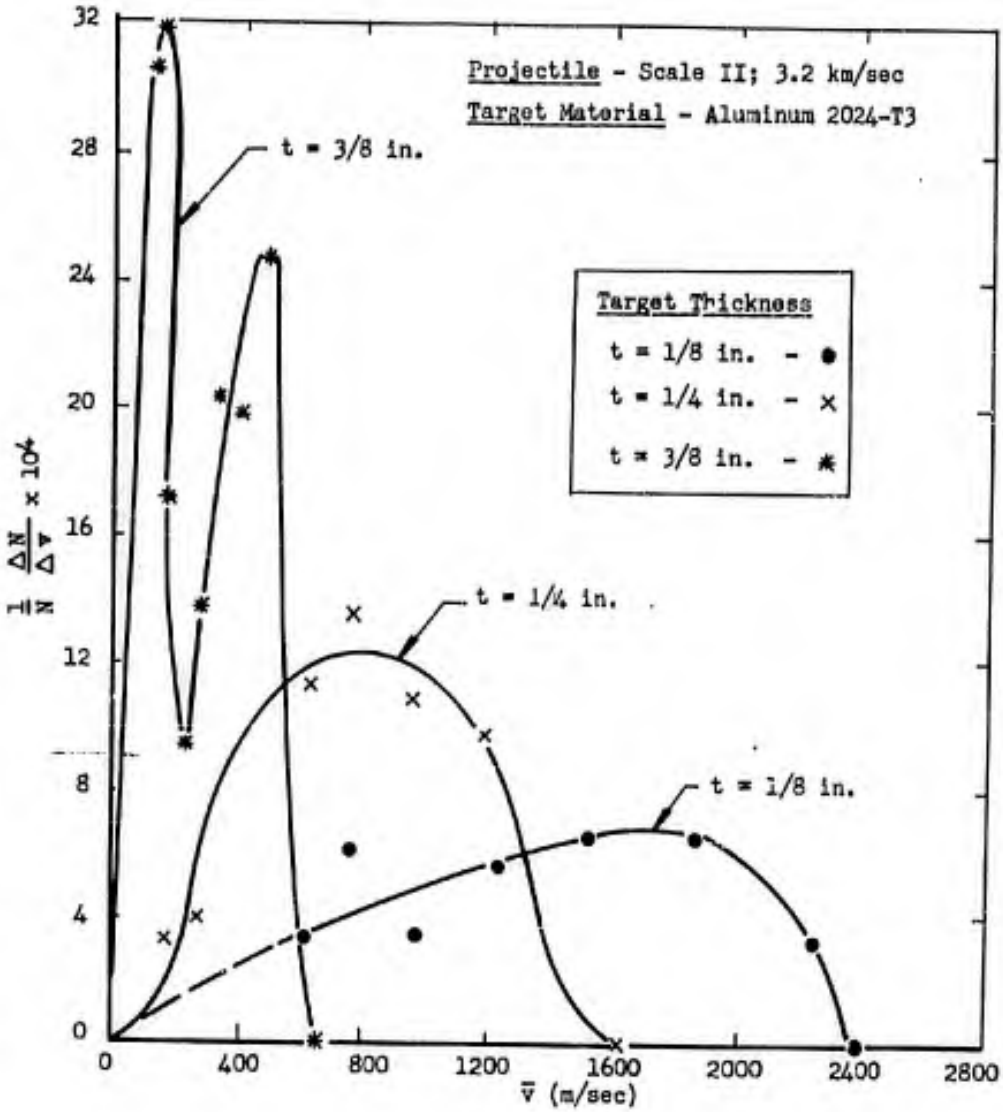

Fig. 4 Plot similar to figure 3 except that only the 20% of the total number of spall particles having the highest penetration capabilities are considered in the distribution in velocity space.

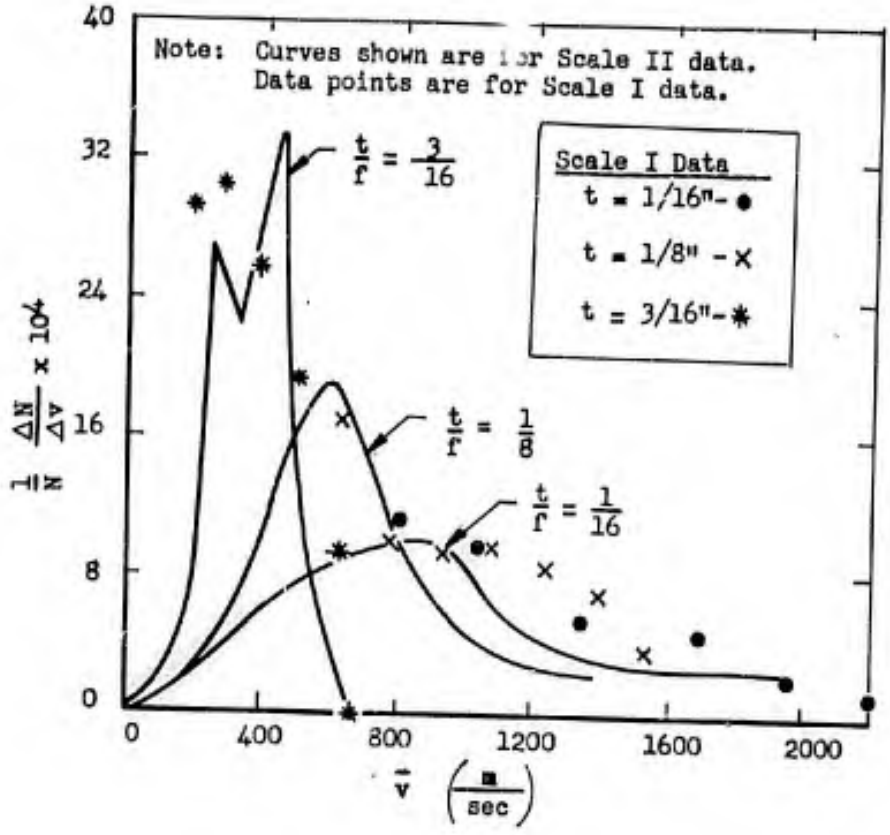

Fig. 5 The probable scaling relationship of the spall velocity distributions for Scale I and Scale II projectiles impacting three thicknesses of 2024-T3 aluminum targets.

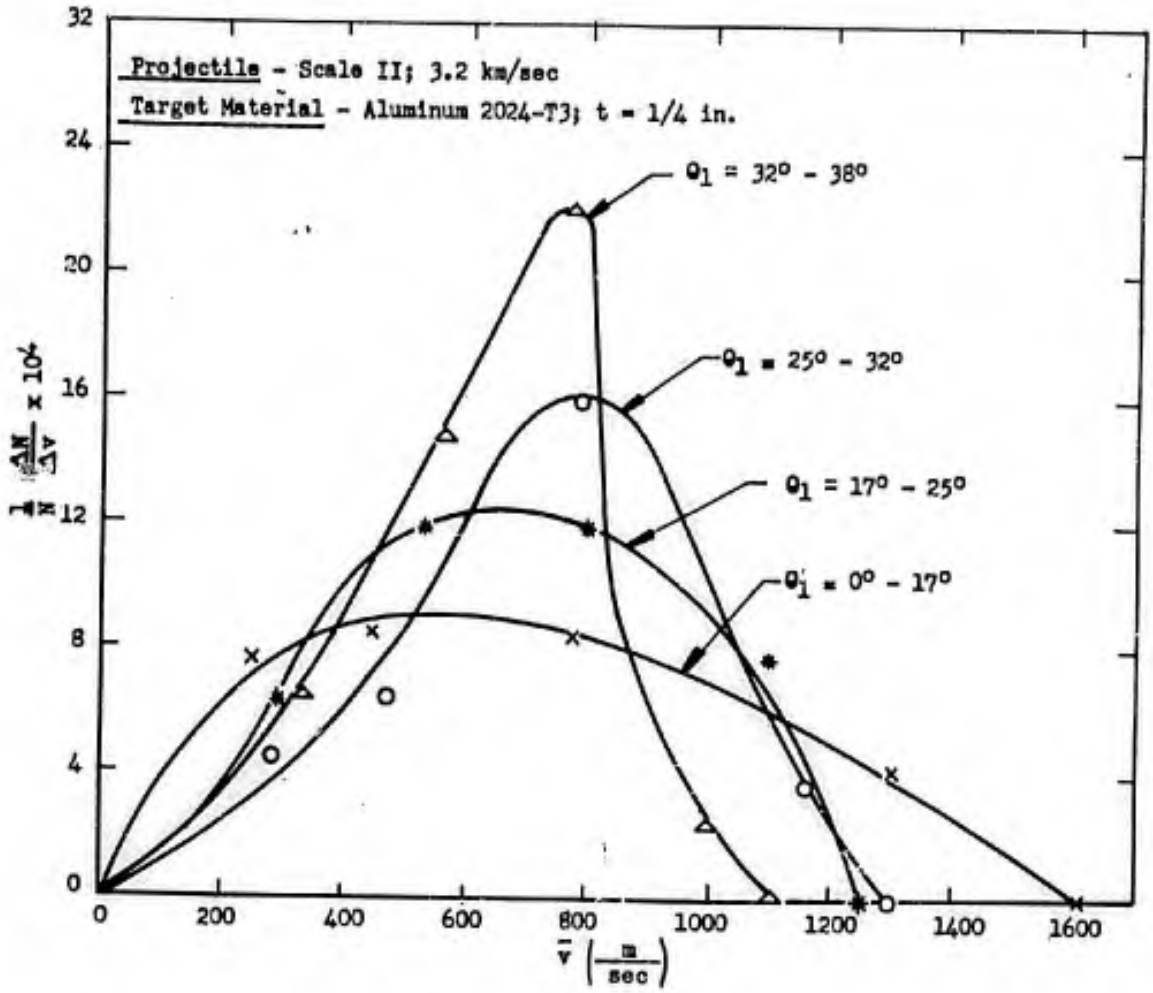

Fig. 6 Comparison of the spall velocity distribution for spall at different radial distances out from the center of spall impact. The plot shows the relative percentage of spall particles residing in various elements of the velocity spectrum.

DISTRIBUTION LIST FOR

Type I Quarterly Report

on

Hypervelocity Impact Phenomena

Sponsored by the Department of the Army
Aberdeen Proving Ground

Commanding General
Aberdeen Proving Ground
Maryland
Attn: F. E. Allison
Ballistic Research Laboratories

Commanding General
Aberdeen Proving Ground
Maryland
Attn: E. J. Eichelberger
Ballistic Research Laboratories

Commanding General
Aberdeen Proving Ground
Maryland
Attn: Technical Library
Ballistic Research Laboratories

Office, Chief of Ordnance
Department of the Army
Washington 25, D. C.
Attn: ORDTU

British Joint Services Mission
1800 K Street, N. W.
Washington 6, D. C.
Attn: Reports Officer

Commanding Officer
U. S. Naval Ordnance Test Station
China Lake, California
Attn: J. W. Rogers

Commanding Officer
Air Proving Ground Center
Eglin Air Force Base, Florida
Attn: H. L. Davis

Commanding General
Aberdeen Proving Ground
Maryland
Attn: S. Kronman
Ballistic Research
Laboratories

Commanding General
Aberdeen Proving Ground
Maryland
Attn: J. Kineke
Ballistic Research
Laboratories

Office, Chief of Ordnance
Department of the Army
Washington 25, D. C.
Attn: ORDTB, Ballistics Section
Mr. M. C. Miller

Commanding Officer
Armed Services Technical Information Agency
Arlington Hall Station
Arlington 12, Virginia
Attn: TIPCR

Canadian Army Staff
2450 Massachusetts Avenue
Washington 8, D. C.

Director
U. S. Naval Research Laboratory
Washington 25, D. C.
Attn: Mr. W. W. Atkins, Code 130

Commanding Officer
Air Proving Ground Center
Eglin Air Force Base, Florida
Attn: Lt. W. H. Dittrich
Det. 4, ASD(ASQWR)

Director, The RAND Corporation
1700 Main Street
Santa Monica, California
Attn: J. H. Huth

Director, The RAND Corporation
1700 Main Street
Santa Monica, California
Attn: R. L. Bjork

Director, The RAND Corporation
1700 Main Street
Santa Monica, California
Attn: Technical Library

Library of Congress
Technical Information Division
Reference Department
Washington 25, D. C.
Attn: Bibliograph Section

General Motors Corporation
Defense Systems Div., Box T
Santa Barbara, California
Attn: J. W. Gehring

Firestone Tire & Rubber Company
1200 Firestone Parkway
Akron, Ohio
Attn: C. M. Cox

Commanding Officer
Air Proving Ground Center
Eglin Air Force Base, Florida
Attn: F. E. Howard
Det. 4, ASD(ASQP)

Director, National Aeronautics &
Space Administration
Ames Research Center
Moffett Field, California
Attn: J. L. Summers

Director, National Aeronautics &
Space Administration
Ames Research Center
Moffett Field, California
Attn: Technical Library

Director, National Aeronautics &
Space Administration
Langley Research Center
Langley Field, Virginia
Attn: W. H. Kinard

Director, National Aeronautics &
Space Administration
Langley Research Center
Langley Field, Virginia
Attn: Technical Library

General Motors Corporation
Defense Systems Div., Box T
Santa Barbara, California
Attn: Technical Library

Aeroelastic & Structures Laboratory
Massachusetts Institute of Tech-
nology
77 Massachusetts Avenue
Cambridge 39, Massachusetts
Attn: W. Herrmann

Drexel Institute of Technology
Mechanical Engineering Dept.
Philadelphia 4, Pennsylvania
Attn: Pei Chi Chou

National Aeronautics and Space
Administration
Lewis Research Center
21000 Brookpark Road
Cleveland 35, Ohio

Int.-BuMines, Pittsburgh, Pa.

UNCLASSIFIED